ACS APPLIED MATERIALS & INTERFACES

Research Article

www.acsami.org

Engineering Vascularized Bone Grafts by Integrating a Biomimetic Periosteum and β-TCP Scaffold

Yunqing Kang,[†,∥] Liling Ren,[†,‡,∥] and Yunzhi Yang*[,†,§]

[†]Department of Orthopedic Surgery, Stanford University 300 Pasteur Drive, Stanford, California 94305, United States

[‡]School of Stomatology, Lanzhou University 199 Donggang West Road, Lanzhou, Gansu 730000, China

[§]Department of Materials Science and Engineering, Stanford University, 300 Pasteur Drive, Stanford, California 94305, United States

Supporting Information

ABSTRACT: Treatment of large bone defects using synthetic scaffolds remain a challenge mainly due to insufficient vascularization. This study is to engineer a vascularized bone graft by integrating a vascularized biomimetic cell-sheet-engineered periosteum (CSEP) and a biodegradable macroporous beta-tricalcium phosphate (β-TCP) scaffold. We first cultured human mesenchymal stem cells (hMSCs) to form cell sheet and human umbilical vascular endothelial cells (HUVECs) were then seeded on the undifferentiated hMSCs sheet to form vascularized cell sheet for mimicking the fibrous layer of native periosteum. A mineralized hMSCs sheet was cultured to mimic the cambium layer of native periosteum. This mineralized hMSCs sheet was first wrapped onto a cylindrical β-TCP scaffold followed by wrapping the vascularized HUVEC/hMSC sheet, thus generating a biomimetic CSEP on the β-TCP scaffold. A nonperiosteum structural cell sheets-covered β-TCP and plain β-TCP were used as controls. In vitro studies indicate that the undifferentiated hMSCs sheet facilitated HUVECs to form rich capillary-like networks. In vivo studies indicate that the biomimetic CSEP enhanced angiogenesis and functional anastomosis between the in vitro preformed human capillary networks and the mouse host vasculature. MicroCT analysis and osteocalcin staining show that the biomimetic CSEP/β-TCP graft formed more bone matrix compared to the other groups. These results suggest that the CSEP that mimics the cellular components and spatial configuration of periosteum plays a critical role in vascularization and osteogenesis. Our studies suggest that a biomimetic periosteum-covered β-TCP graft is a promising approach for bone regeneration.

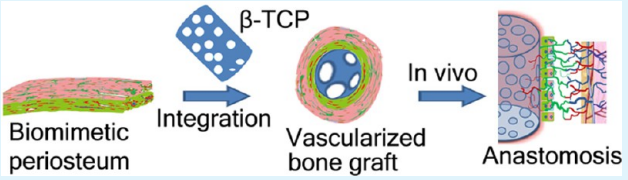

KEYWORDS: *β-TCP, biomimetic periosteum, cell sheet, vascularization, osteogenesis, bone tissue engineering*

1. INTRODUCTION

Current treatments of bone reconstructions in orthopedic and craniomaxillofacial surgery,[1] including autografts and allografts, are limited by either donor tissue availability, morbidity, and infection of second surgery or immune rejection risks.[2,3] Many studies have used synthetic bioceramic scaffolds as an alternative for the repair of bone defects.[4−8] However, the repair and reconstruction of synthetic bone grafts for large bone defects remain challenge due to insufficient vascularization in addition to limited osteoinductivity and osteogenesis in vivo once implanted.[9−11] To overcome this problem, several approaches were developed to increase the rate of vascularization in a scaffold after implantation, including the loading of growth factors (such as VEGF, PDGF) on an implanted bone scaffold,[12−15] monoculture of endothelial cells, and coculture of endothelial cells and bone-forming cells,[16−19] or inserting a vascular bundle in scaffolds.[20,21] However, these approaches still suffer from insufficient neo-vascularization in the scaffolds and a slow invasion rate of host vasculature in vivo or anastomosis for large bone grafts. Therefore, a new strategy for accelerating vascularization and functional anastomosis is still highly desirable.

Periosteum has an important role in bone regeneration.[22] Periosteum is a membrane that covers the outer surface of bones. It mainly consists of distinct two layers: an outer fibrous layer and inner cambium layer. The fibrous layer contains collagen, fibroblasts, and blood vessels that provide nourishment to the inner bone, while the inner cambium layer contains progenitor cells that provide a rich source of osteogenic cells for the healing of bone fractures.[23−25] Studies have indicated that periosteum can increase the rate and quantity of bone formation and improve the vascular invasion ability in large segmental defects.[26] If a vascularized periosteal sleeve is present, more vessel invasion and thus bone formation in an implanted bone graft can be achieved.[27,28] In the absence of periosteum, bone resorption often occurs.[29] However, the supply of autograft periosteum is limited.[30−32] To overcome the limitation of autograft periosteum, synthetic tissue-engineered periostea have been developed, using osteoinduced rabbit bone marrow mesenchymal stem cells (MSCs) and porcine small intestinal submucosa (SIS),[33] or using an acellular human dermis, which is capable of

Received: April 4, 2014
Accepted: May 23, 2014
Published: May 23, 2014

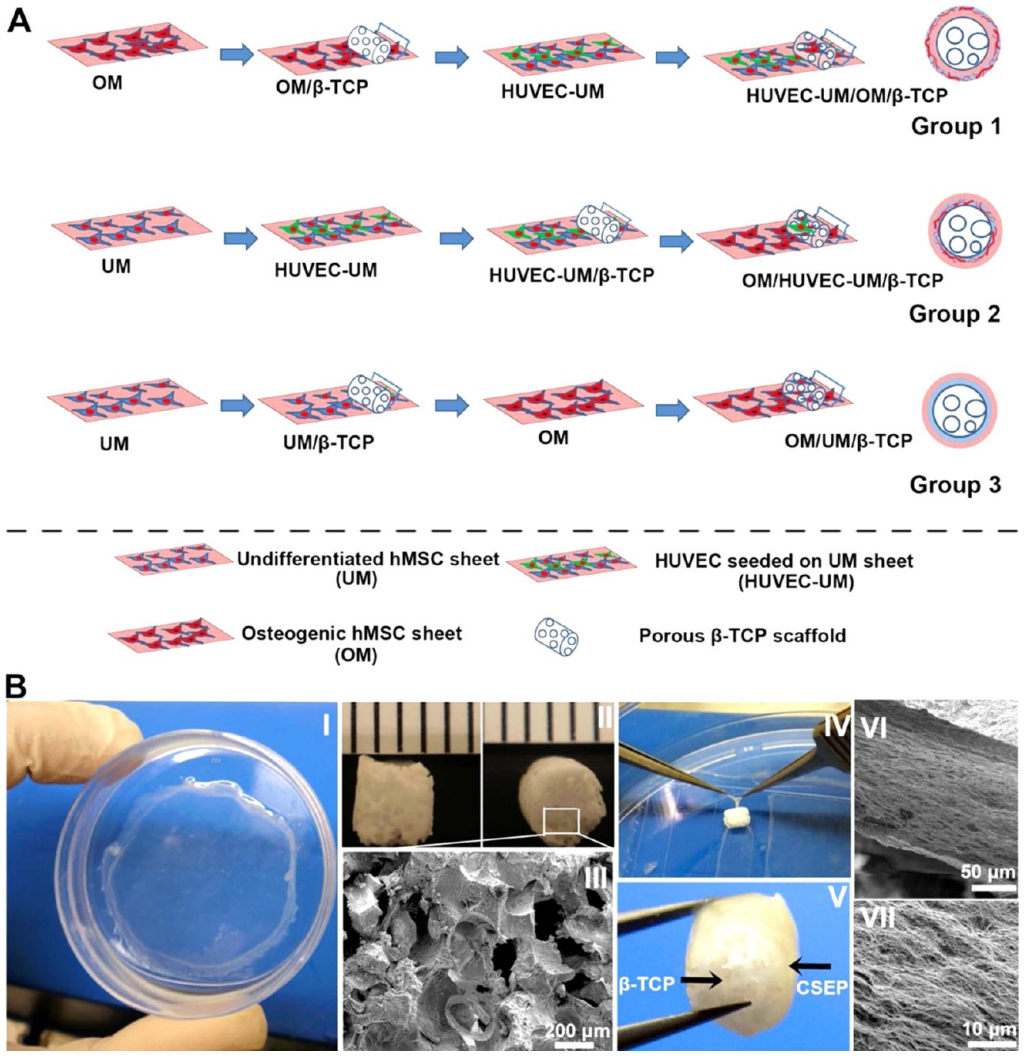

Figure 1. Step-by-step procedures for preparing cell sheet/β-TCP composite grafts. Preparing three cell sheet/β-TCP grafts including OM/UM/β-TCP, OM/HUVEC-UM/β-TCP, and HUVEC-UM/OM/β-TCP (A). (B) Macroscopic view of an hMSCs sheet on a dish (I) and a porous β-TCP scaffold (II). SEM image demonstrates the morphology of β-TCP pores (III). Point forceps were used to wrap the cell sheet onto a β-TCP scaffold (IV), thus generating a HUVEC-UM/OM/β-TCP graft (V). SEM images show a very dense extracellular matrix of cell sheet on a β-TCP scaffold (VI, VII).

supplying cells and osteoinductive proteins.[34] However, these tissue-engineered periostea demonstrated limited vascularization ability. Recent studies have reported the significant progress in engineered periostea by corporating MSCs into hydrogel or decelluralized allografts.[35−39] However, developing a novel tissue-engineered periosteum with high vascularization ability and similar function and structure of native periosteum would be still needed, and it should enhance the vascularization and osteogenesis ability of an implanted graft.

In this study, we used a new strategy for boosting vascularization of an implanted bone graft through constructing a biomimetic cell-sheet-engineered periosteum (CSEP) and combining it with a biodegradable porous beta-tricalcium phosphate (β-TCP) scaffold. We hypothesized that the prevascularized biomimetic CSEP can promote the vascularization of the porous β-TCP scaffold and that the porous scaffold can provide structural support to the CSEP during handling and implantation. To this end, we used hMSCs and HUVECs as cell sources to form relevant cell sheets which mimic the fibrous layer and cambium layer of native periosteum. The hMSCs was chosen to form cell sheet matrix due to its stabilization ability for new-formed blood vessels as a pericyte and the osteogenic differentiation potential.[40,41] HUVECs were seeded on an undifferentiated hMSCs sheet (UM) to generate a prevascularized cell sheet (HUVEC-UM, biomimetic fibrous layer), and hMSCs were also cultured in osteogenic medium to form an osteogenic mineralized cell sheet (OM, biomimetic cambium layer). We first detached and wrapped the OM cell sheet onto a β-TCP scaffold followed by a prevascularized HUVEC-UM cell sheet, thus generating a biomimetic CSEP on the β-TCP scaffold (mostly like periosteum-covered bone structure). We fabricated three groups of double cell sheet layers with β-TCP scaffolds: Group 1 contained an outer HUVEC-UM layer and inner OM layer that is in contact with the β-TCP core (HUVEC-UM/OM/β-TCP, periosteum/bone-like group); Group 2 contained an outer OM layer and an inner HUVEC-UM layer that is in contact with the β-TCP core (OM/HUVEC-UM/β-TCP, nonperiosteum/bone-like group); and Group 3 contained an outer OM layer and an inner nonprevascularized UM layer (OM/UM/β-TCP, nonprevascularized group). Group 4 was the plain β-TCP scaffolds without any cell sheets wrapped. In vitro prevascularization ability and in vivo animal studies were performed to characterize the vascularization and osteogenic potentials of these grafts.

dx.doi.org/10.1021/am502056q | ACS Appl. Mater. Interfaces 2014, 6, 9622−9633

2. MATERIALS AND METHODS

2.1. Preparation of Porous β-TCP Scaffolds. A template-casting method, as previously described, was used to prepare the porous β-TCP scaffolds.[42] Briefly, a β-TCP ceramic slurry was prepared through mixing β-TCP powder, carboxymethyl cellulose powder, surfactant (Surfonal), and dispersant (Darvan C) in distilled water. A 96 well plate was used as a mold to load paraffin beads and heated to form a template. The β-TCP ceramic slurry was then cast into the mold and subsequently dehydrated in a series of ethyl alcohol solutions. After removal of the dehydrated green body from the mold, the green body was sintered in an electric high temperature furnace at 1250 °C for 3 h. The pore morphology of the β-TCP scaffolds was characterized by scanning electron microscopy. The average porosity of the scaffold fabricated by this method is around 80%.[43−45] The scaffolds used in this study were about 3 mm in diameter and around 4 mm in length.

2.2. Cell Culture. hMSCs from Lonza Inc. (Allendale, NJ) were cultured in basal media consisting of Dulbecco's Modified Eagle media (DMEM, Invitrogen, U.S.A.) with 10% FBS, 1% L-glutamine (200 mM), 1% antibiotic-antimycotic solution under standard conditions (5% CO_2, 95% humidity, and 37 °C). Passage 6−9 of hMSCs was used for all the experiments in this study. HUVECs constitutively expressing GFP were a generous gift from the late Dr. J. Folkman, Children's Hospital, Boston.[43] HUVECs were cultured in endothelial basal medium (EBM-2, Lonza) with endothelial growth supplement SingleQuots (EGM-2, Lonza) in a 5% CO_2 atmosphere at 37 °C.

2.3. Production of Prevascularized Cell Sheet. To engineer a prevascularized cell sheet in vitro, hMSCs were seeded on a cell culture dish at a cell density of $9 \times 10^4/cm^2$ and cultured in DMEM undifferentiated medium. After cells reached confluence, the DMEM medium received an addition of 50 μg/mL ascorbic acid and 30 mM glucose, which promotes the production of extracellular matrix. After 14 days of culture, undifferentiated hMSCs can form a thick cell sheet layer that was designated as UM. Then, a cell suspension of HUVECs was seeded onto the surface of the UM sheet at a cell density of $5 \times 10^4/cm^2$. Afterward, EBM-2 culture medium was added to the growing cells for 7 days. Medium was changed every 3 days.

2.4. Immunofluorescent Staining of HUVEC-UM Cell Sheet. To characterize the HUVECs on the UM sheet (HUVEC/UM), immunofluorescent staining was performed. Expression of platelet-endothelial cell adhesion molecule (PECAM-1, or CD31), an endothelial-specific adhesion protein of HUVECs, was assessed by immunofluorescent staining. At the end of days 3, 5 and 7, the HUVEC-UM sheets were washed three times in PBS. A 5% goat serum-PBS buffer solution was used to block the cell sheet samples for 1 h at room temperature, and then primary antibody mouse antihuman CD31 (89C2, Cell Signaling Technology, dilution 1:3200) in 1% BSA-PBS was added into the sample, followed by incubation overnight at 4 °C. After washing with PBS, a secondary antibody goat−antimouse (Alexa Fluor 594, Invitrogen, 2 μg/mL) in 1% BSA-PBS was added and incubated in the dark for 1 h at room temperature. Finally, the cell nuclei were counterstained with DAPI (5 μg/mL) for 1 min and then extensively washed with PBS. The fluorescent staining was imaged by fluorescent microscopy (Zeiss). All 3-dimensional images taken by confocal microscope were reconstructed using Volocity software.

2.5. Production of Osteogeneic Cell Sheet. Besides producing the prevascularized HUVEC-UM sheet, an osteogenic hMSCs sheet (designated OM) was fabricated at the same time. hMSCs were cultured in osteogenic medium containing 10% FBS, 10 mM β-glycerophosphate, 10 nM dexamethasone, and 50 μg/mL ascorbic acid and 30 mM glucose for 21 days. To characterize the osteogenic properties, alizarin red staining and von Kossa staining were performed.

2.6. Production of Cell Sheet/β-TCP Complex. To obtain biomimetic periosteum-covered β-TCP scaffolds, an OM sheet strip (around 5 mm width and 60 mm length) was cut in a 100 mm culture dish, and then, a porous β-TCP scaffold was placed on the OM sheet strip. The OM cell sheet was then detached by sharp pointed forceps, lifted, and wrapped onto the scaffold via rolling. Afterward, a prevascularized HUVEC-UM strip (around 5 mm width and 60 mm length) was also cut in an another 100 mm culture dish. The OM-covered scaffold was then placed onto this prevascularized HUVEC-UM strip. This HUVEC-UM layer was then wrapped via rolling onto the OM/scaffold. Thus, a biomimetic prevascularized periosteum was formed on the porous β-TCP scaffold. For comparison, a reverse structural membrane (first wrapping HUVEC-UM sheet on the β-TCP and then OM sheet was wrapped on the HUVEC-UM-covered β-TCP) was fabricated using the same method. As controls, a nonprevascularized OM/UM sheet-covered β-TCP group (without HUVECs) and a scaffold-only group were also prepared. A schematic graph in Figure 1 illustrates the procedure and related names of groups. To obtain the same layer number of the rolled cell sheets on the scaffold, the width and length of each cell sheet were kept same in all the groups (Figure1).

2.7. Cell Migration. To investigate whether cells can migrate from the cell sheet into the scaffold, the HUVEC-UM/OM/β-TCP complex was fixed with 4% paraformaldehyde after 3, 7, and 14 days of culture and stained with DAPI (5 μg/mL) for 1 min. The fluorescent staining was imaged by fluorescent microscopy (Zeiss). Scanning electronic microscope (SEM) was also used to observe the migration of cells from the peripheral cell sheet into the center of the scaffold. At the designated time points, the graft was fixed by 2.5% glutaraldehyde and sequentially dehydrated in aqueous solutions of increasing ethanol concentrations. A FEI XL30 Sirion SEM was used to observe cells on the scaffolds after the composite scaffolds were coated.

2.8. In Vivo Implantation. Four groups including HUVEC-UM/OM/β-TCP, OM/HUVEC-UM/β-TCP, OM/UM/β-TCP, and plain β-TCP scaffolds were prepared for in vivo implantation. The grafts were subcutaneously implanted in nude mice. In this study male immunodeficient nude mice (6−7 week old, 20−25 g body weight, Charles River Laboratories, Sulzfeld, Germany) were used for all surgeries. Four groups were implanted into four separate subcutaneous dorsal pockets per animal. 25 μg cefazolin/g and 0.1 μg buprenorphine/g mouse were administrated, and after surgery, one mouse per cage was housed. This in vivo animal study was approved by the Administrative Panel on Laboratory Animal Care (APLAC) of Stanford University. Each experimental time point and condition was replicated in 4 mice. Implants were harvested after 2, 4, and 8 weeks for histological analysis.

2.9. Histology and Immunohistochemistry Staining. After 2, 4, and 8 weeks, the mice were euthanized and the implants were retrieved, fixed in buffered formalin (10%) for 24 h, and decalcified in 50 mM EDTA for 1 week. The EDTA solution was changed every day. After extensive washing, the decalcified complex was gradually dehydrated in ethanol solutions and embedded in paraffin, and 7 μm-thick sections were sliced. To show the presence of luminal structures containing red blood cells, conventional hematoxylin and eosin (H&E) staining was carried out on paraffin sections. The microvessels formed in the grafts in vivo were quantified by evaluation of 8 random fields (under 40× magnification) of H&E stained sections from four individual mice. The luminal structures containing red blood cells were defined as microvessels. The density of these microvessels was reported as the average number of erythrocyte-filled microvessels per mm^2 and expressed as mean values ± the standard deviation. For investigating whether the prevascularized human blood vessels in vitro can be anastomosed with host vasculature in vivo, immunohistochemistry of human anti-CD31 were performed. To further confirm the migration or proliferative survival of implanted human cells in vivo, immunohistochemistry staining of antihuman vimentin was also performed. Sections were deparaffinized and unmasked by an antigen retrieval solution at 95−100 °C, and then, the sections were blocked by goat blocking serum (5%) for 30 min. Rabbit antihuman CD31 antibody (Clone EP3095 for human microvessel detection; 1:500; Millipore) and mouse antihuman vimentin antibody (ab8069, 1:400, abcam) were used. Biotinylated goat antirabbit and antimouse secondary antibodies (1:200; Vector Laboratories) and DAB substrate kit (Vector Laboratories) were used, followed by hematoxylin counterstaining and permanent mounting. An intact CD31-expressing lumen containing red blood cells was defined as a functional perfused blood vessel anastomosed with host vasculature. The density of this kind of lumen was reported as the average number of $CD31^+$ lumen per mm^2 and expressed as mean values ± the standard deviation (n = 4).

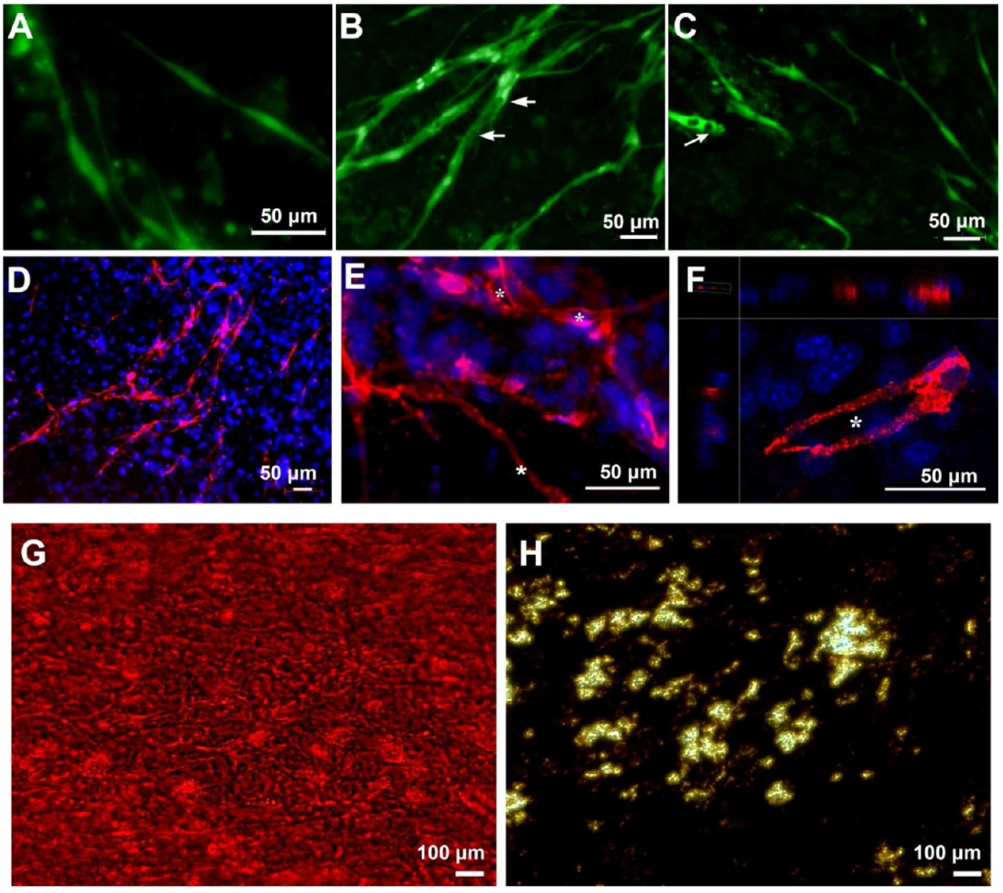

Figure 2. HUVECs on an undifferentiated hMSCs sheet formed numerous networks. Networks started at day 3 (A), and elongated to form many lumens at day 5 (B) and day 7 (C). Arrows indicate lumens. Immunofluorescent staining images of CD31 show several networks on the hMSCs sheet at day 7 (D, 10× magnification; E, 20× magnification); 3D-reconstructed confocal images display lumen formation (F). Asterisks show the lumens. Alizarin red staining (G) and vov Kossa staining (H) show the mineralized matrix of osteogenic hMSC cell sheet.

2.10. Osteogenesis Assays. Microcomputed tomography (MicroCT; Imtek MicroCAT II; Knoxville, TN) at a resolution of 80 μm was used to scan the change in bone volume with implantation time. Live mice were scanned at 2, 4, and 8 weeks. Images were further analyzed by GE MicroView2.2 (General Electric Co.). The gray threshold value of the samples at week 2 was used as the starting time point. Based on this threshold, the Hounsfield Units (HU) of the same samples in the same mouse at the designated time points was calculated. The increase percentage of the HU at 4 and 8 weeks is designated as the increase volume ratio of the newly formed bone and the degradation of the scaffold, related to 2 weeks (n = 4) (see Supporting Information).

To further identify the osteogenic capability of the grafts, immunohistochemistry staining of osteocalcin and tartrate-resistant acid phosphatase staining (TRAP) of osteoclast activity were carried out on paraffin sections.

2.11. Statistical Analysis. All the values were reported as mean values ± SD and statistically analyzed using one-way ANOVA analysis. If the p-value obtained from the test was less than 0.05, the difference was considered statistically significant.

3. RESULTS

3.1. Fabrication of the Cell Sheet/Scaffold Grafts. Figure 1 shows the schematic for making the cell-sheet/β-TCP scaffold. Four groups of samples, including HUVEC-UM/OM/β-TCP, OM/HUVEC-UM/β-TCP, OM/UM/β-TCP, and plain β-TCP scaffolds, were prepared (Figure 1A). Figure 1B shows the entire process of fabrication, including a cell sheet (Figure 1B, I), a scaffold (Figure 1B, II and III), the wrapping (Figure 1B, IV) and the final graft (Figure 1B, V). SEM observation indicates that the cell sheets had an enriched extracellular matrix (ECM) after 14 days of incubation (Figure 1B, VI and VII).

3.2. Characterization of the Vascularized Cell Sheet and Mineralized Cell Sheet. Immunofluorescent staining of CD31 was performed to investigate the in vitro angiogenesis of the HUVEC-UM sheet. Fluorescent images in Figure 2 indicate a progressive capillary morphogenesis. At an early stage (day 3), the HUVECs connected and aligned with each other and formed networks (Figure 2A). With time, the networks became rich. A large number of vacuoles formed at day 5 (Figure 2B) and day 7 (Figure 2C). The presence of cell-lined lumens was further investigated by confocal microscopy examination (Figure 2D–F). The confocal images show the establishment of a large number of lumens at day 7 (Figure 2D and E). 3D reconstructed image further indicates that the formation of lumen structures (Figure 2F). These results indicate that the hMSCs sheet provides a suitable environment for cell-mediated formation of lumen-containing capillary networks in vitro. Alizarin red staining and vov Kossa staining results show the formation of mineralized matrix in the osteogenic cell sheet (Figure 2G and H).

3.3. Cell Migration from Outer Cell Sheet to Inner Scaffold. We further studied cell migration from the peripheral cell sheet into the scaffold. After the cell sheets were wrapped on the scaffolds and cultured for 3, 7, and 14 days, the cell sheet/scaffold grafts were fixed and stained by DAPI (Figure 3A). The DAPI stained all the cells, including hMSCs and green

dx.doi.org/10.1021/am502056q | ACS Appl. Mater. Interfaces 2014, 6, 9622–9633

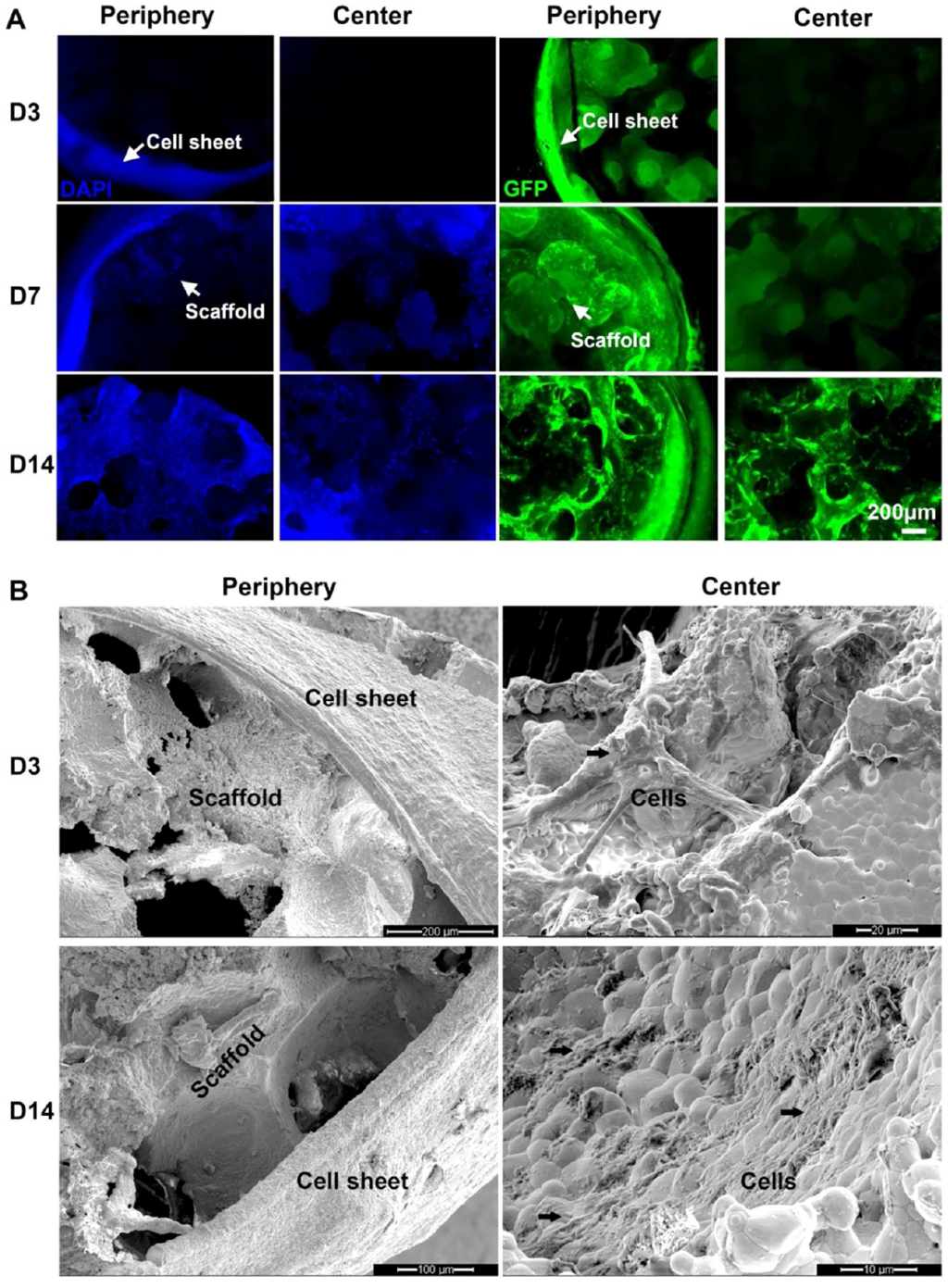

Figure 3. Fluorescent images of DAPI staining, GFP-HUVECs, and SEM images show cell migration. Cells migrated into the periphery of the scaffold but did not reach its center at day 3. With time, cells started to migrate further from the periphery toward the center at 7 days and 14 days (A); SEM images show a very dense cell sheet wrapped on the β-TCP scaffold and the morphology of ECM. Cells migrated from the peripheral cell sheet into the β-TCP scaffold at day 3 and day 14 (B).

fluorescent protein-tagged HUVECs (GFP-HUVECs). GFP fluorescent images show the migration of HUVECs. All the fluorescent images show that cells in peripheral cell sheets migrated into the pores of the scaffold along the struts of scaffolds with time. At day 3, cells were seen on the peripheral struts closer to the cell sheet. However, in the central region of the scaffolds, there were no cells present. After 7 days, many cells migrated into the inner struts of the scaffold. At day 14, many cells appeared on the struts of both peripheral and central areas (Figure 3A). These results suggest that cells migrated from the cell sheet into the pores and spread into the inner struts of the scaffolds. SEM results confirm this migration (Figure 3B). SEM images also show the cell sheet with rich ECM surrounding the scaffolds, and the cells resided on the inner struts of the scaffolds.

3.4. Vascularization of Cell-Sheet/Scaffolds In Vivo. Hematoxylin/eosin (H&E) staining reveals that the formation of blood vessels in the implants varies among the four groups (Figure 4). A blood vessel is defined as a lumen containing erythrocytes. In the plain scaffold group, few blood vessels were seen. Few cells from the host tissue infiltrated into the pores of

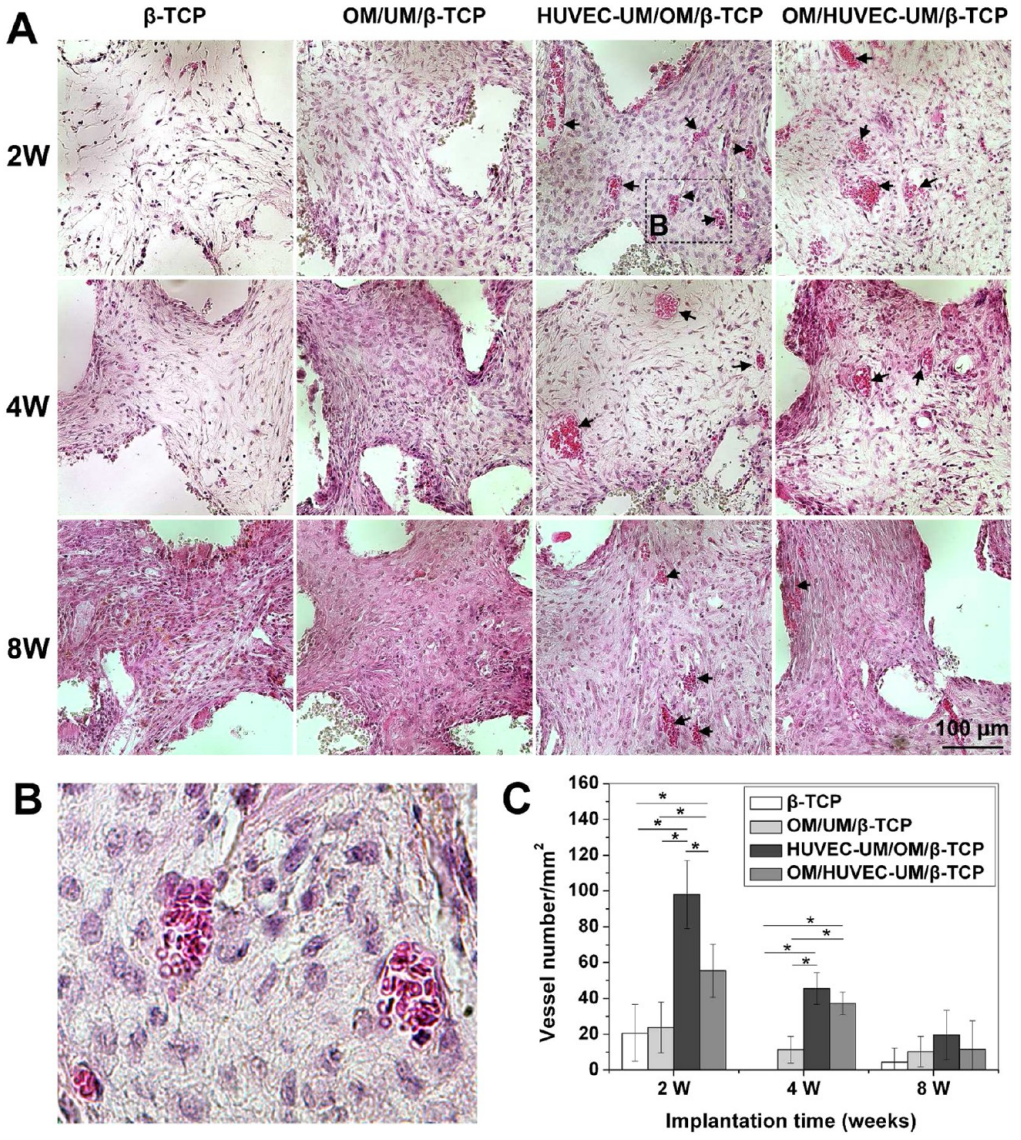

Figure 4. H&E staining results reveal that cells grew into the β-TCP scaffold and OM/UM/β-TCP groups at 2, 4, and 8 weeks, but few blood vessels were observed. However, many blood vessels containing red blood cells were seen in prevascularized groups, HUVEC-UM/OM/β-TCP and OM/HUVEC-UM/β-TCP (A). Magnified image from HUVEC-UM/OM/β-TCP group at 2 weeks shows murine blood cells in a blood vessel lumen (B). A quantitative assay shows the microvessel densities of fours groups at 2, 4, and 8 weeks (* $p < 0.05$, $n = 4$) (C).

the scaffold at 2 weeks after implantation, but at 4 and 8 weeks, more cells penetrated into the scaffold pores (Figure 4A). In the OM/UM/β-TCP group, more cells grew into the pores of the composite scaffolds compared to the plain scaffold group, probably both host cells and human cells from the cell sheet. Similarly to the plain scaffold group, few blood vessels were seen (Figure 4A). However, in the HUVEC-UM/OM/β-TCP group, a higher vessel density was observed. Numerous blood vessels containing erythrocytes were uniformly distributed throughout the implants at 2, 4, and 8 weeks. Compared to that in the HUVEC-UM/OM/β-TCP group, the blood vessels in the OM/HUVEC-UM/β-TCP group were sparsely distributed. A magnified image from HUVEC-UM/OM/β-TCP group in Figure 4A clearly shows that the blood vessel lumen contains many blood cells (Figure 4B). Quantification of blood vessels shows that at 2 weeks after implantation, the vessel density of OM/UM/β-TCP groups without prevascularization (24 ± 14 vessels/mm^2) is slightly higher than that in the plain scaffold (20 ± 16 vessels/mm^2), and that the periosteoum-like HUVEM-UM/OM/β-TCP group has significantly higher density of blood vessels in the implants (98 ± 19 vessels/mm^2) compared to that in the OM/HUVEC-UM/β-TCP group (55 ± 15 vessels/mm^2) (Figure 4C). At 4 weeks after implantation, the vessel density of the periosteum-like HUVEM-UM/OM/β-TCP group (45 ± 9 vessels/mm^2) is still slightly higher than that in the OM/HUVEC-UM/β-TCP group (37 ± 6 vessels/mm^2), and the vessel densities of these two prevascularized groups are significantly higher than those in nonprevascularized and plain scaffolds ($p < 0.05$). However, the difference in the vessel densities of the four groups continues to decrease over time. At 8 weeks after implantation, there is no significant difference among the four groups (Figure 4C).

3.5. Anastomosis of Preformed Networks with Host Vasculature. The formation of functional perfusable blood vessels was evaluated by immunohistochemistry staining of human CD31 (hCD31). The microvessels stained positive for hCD31 and those containing murine erythrocytes were counted to be functional perfusable blood vessels. Human CD31-positive

dx.doi.org/10.1021/am502056q | ACS Appl. Mater. Interfaces 2014, 6, 9622−9633

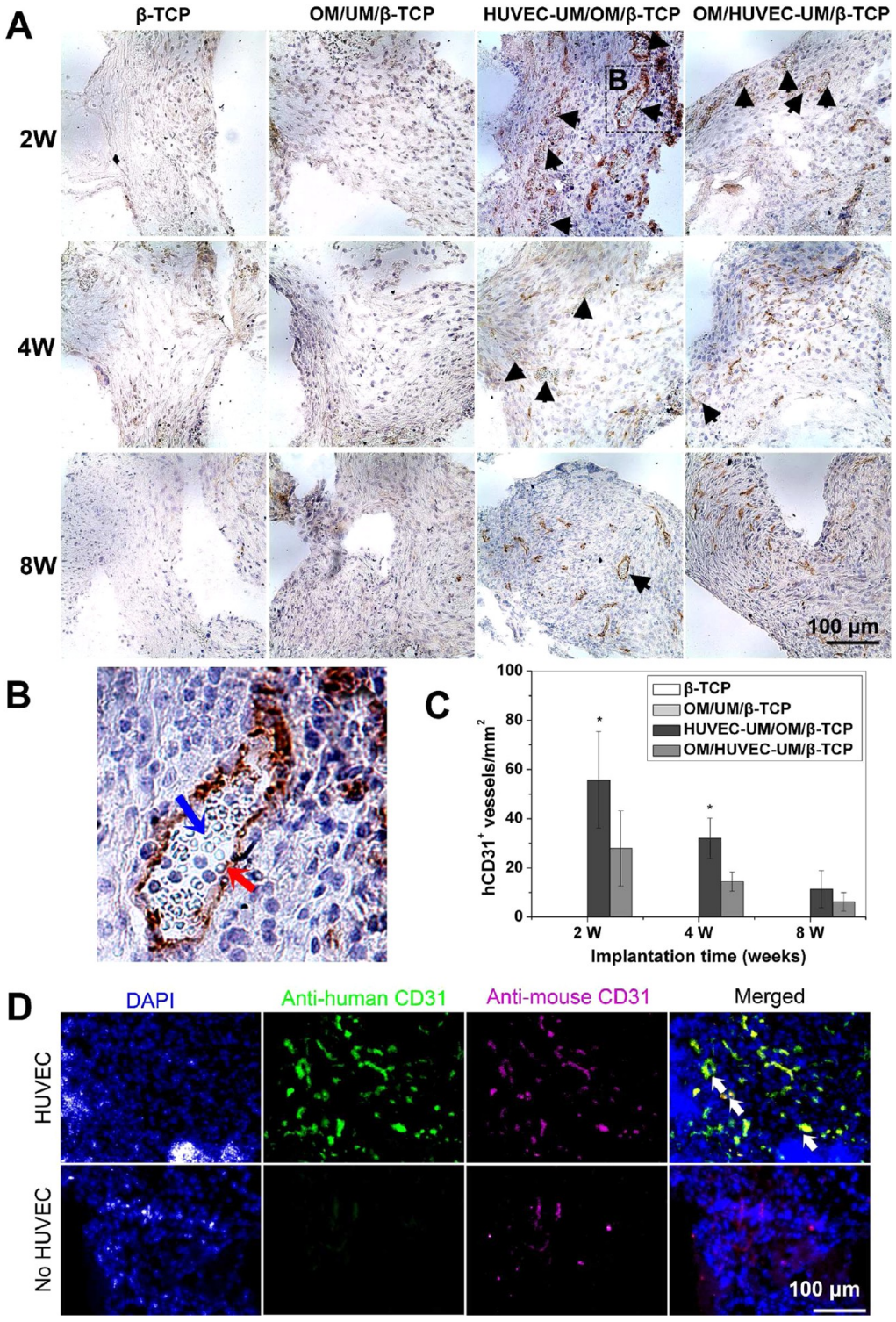

Figure 5. Immunohistochemistry staining of human CD31 shows that many antihuman CD31 positive-expressing lumens were seen in HUVEC-UM/OM/β-TCP and OM/HUVEC-UM/β-TCP (black arrows), but there was no expression in plain β-TCP scaffolds and the nonprevascularized OM/UM/β-TCP group (A). A magnified image from HUVEC-UM/OM/β-TCP group at 2 weeks shows that the preformed human blood vessel lumen (brown color, red arrow) carried murine blood cells (semitransparent round ball, blue arrow) (B). The density of the CD31 positive-expressing lumens was higher in HUVEC-UM/OM/β-TCP than that in OM/HUVEC-UM/β-TCP at 2, 4, and 8 weeks (* $p < 0.05$, $n = 4$) (C). Immunofluorescent double staining shows the expressions of antihuman CD31 (green) and antimouse CD31 (magenta) in nonprevascularized and prevascularized scaffold group. The overlap or partial overlap of the two colors implies the anastomosis of the preformed human capillaries with the host vasculature (yellow, white arrow) (D).

lining lumens were identified as blood vessels formed by implanted human HUVECs. Lumens with negative hCD31 expression were identified as invading murine blood vessels. In the β-TCP and the OM/UM/β-TCP groups, there is no hCD31-positive expression (Figure 5A). In the HUVEC-UM/OM/β-TCP group, numerous lumens containing murine erythrocytes

dx.doi.org/10.1021/am502056q | ACS Appl. Mater. Interfaces 2014, 6, 9622−9633

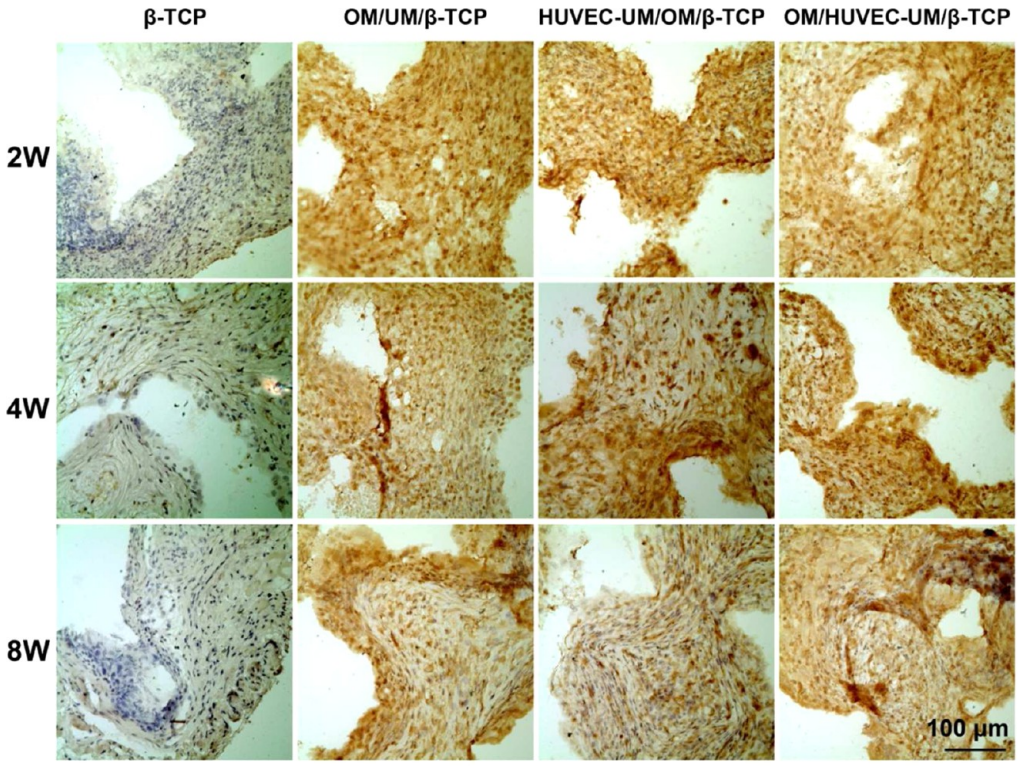

Figure 6. Immunohistochemistry staining of antihuman vimentin shows that many positive-expressing human cells were seen in cell sheet/β-TCP groups from 2 weeks, 4 weeks, to 8 weeks. Human cells migrated from cell sheet to the inner core of β-TCP scaffolds. Host mouse cells (negative expression) also migrated into the plain β-TCP scaffolds.

are observed at 2 weeks after implantation (Figure 5A). At 4 and 8 weeks after implantation, these intact lumens carrying erythrocytes are still seen, but the density decreases. For the OM/HUVEC-UM/β-TCP group, at 2 weeks after implantation, intact lumens containing murine erythrocytes are also apparent, but the number is significantly lower than that in the HUVEC-UM/OM/β-TCP group (Figure 5A). A magnified image of HUVEC-UM/OM/β-TCP group in Figure 5A clearly shows that an intact human lumen contains murine erythrocytes (Figure 5B). Quantification of the microvessel density of hCD31 positive-expressing lumens reveals statistically significant differences between the HUVEC-UM/OM/β-TCP group (61 ± 24 vessels/mm^2) and the OM/HUVEC-UM/β-TCP group (26 ± 20 vessels/mm^2) at 2 and 4 weeks (Figure 5C). These results prove that prevascularized cell sheets were able to form extensive vascular networks in vivo and that those prevascularized networks could anastomose with the mouse vascular system and functionally deliver blood. Furthermore, the HUVEC-UM/OM/β-TCP group with biomimetic periosteum-like structure could form notably more functional blood vessels, compared to the OM/HUVEC-UM/β-TCP group (nonperiosteum-like structure) ($p < 0.05$, Figure 5C). Double immunofluorescence staining with antihuman CD31 and antimouse CD31 indicates that there are positive expressions of mouse CD31 in the nonprevascularized scaffold group (Figure 5D) but there are not expressions of human CD31. In prevascularized scaffold groups, both of human and mouse CD31 positive expression were observed. Some overlap points or lumens where both human and mouse CD31were present can be seen in the periosteum-like groups, which suggested that the preformed blood vessels anastomosed with the host vasculature. These results validate our hypothesis that the prevascularized periosteum-like structural cell-sheet layer significantly promotes the formation of functional microvessels within the graft.

A specific antihuman vimentin antibody was used to indicate the survival and migration of human cells from the implanted engineered cell sheet into the inner β-TCP scaffold. Results of immunohistochemistry staining show that vast number of human cells migrated into the entire area of the scaffolds (Figure 6). β-TCP alone group shows that host mouse cells migrated into the pores of the scaffold (negative antihuman expression). These results indicate that macropores of the scaffold facilitate the cell migration and further functional tissue development.

3.6. Evaluation of Ectopic Osteogenesis In Vivo. Figure 7 shows the change of mineral content of the implanted cell-sheet/scaffolds. Micro-CT analysis indicates that the mineral volume of the plain scaffolds significantly decreased during the period of 8 weeks because of biodegradation. At 8 weeks after implantation, the mineral volume of the β-TCP scaffold decreased by $12.83 \pm 0.05\%$ of its original mineral content. For both the OM/UM/β-TCP and OM/HUVEC-UM/β-TCP groups, there was a slight decline in the total mineral volume during the period of 8 weeks. This suggests that the rate of calcification of new osteoid matrix was slightly slower than the degradation rate of the scaffolds. However, in the HUVEC-UM/OM/β-TCP group, there is significant increase in total mineral volume over time. The mineral volume increases $2.24 \pm 0.02\%$ at 4 weeks after implantation and $5.50 \pm 0.02\%$ at week 8. This result suggests that there is a greater quantity of new calcified osteoid matrix than the degradation of the scaffold.

Immuohistochemistry staining of osteocalcin further indicates more bone matrix in the HUVEC-UM/OM/β-TCP and OM/HUVEC-UM/β-TCP groups than other groups at 2, 4, and 8 weeks after implantation (Figure 8A). Tartrate-resistant acid

dx.doi.org/10.1021/am502056q | ACS Appl. Mater. Interfaces 2014, 6, 9622−9633

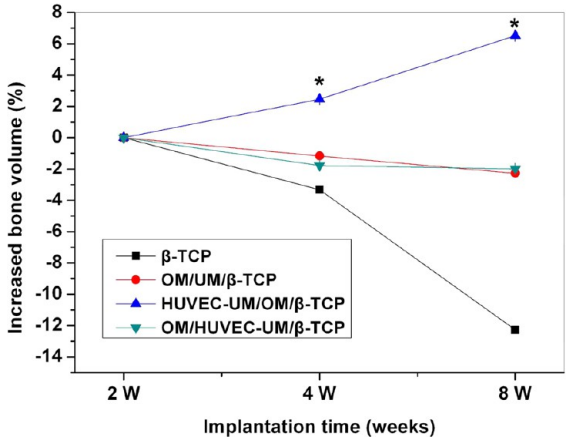

Figure 7. Quantitative assay shows that HUVEC-UM/OM/β-TCP induced higher bone volume than all other groups at 4 and 8 weeks (* $p < 0.05$, $n = 4$).

phosphatase staining (TRAP) staining shows the positive activities of osteoclasts in HUVEC-UM/OM/β-TCP and OM/HUVEC-UM/β-TCP groups, but no osteoclasts activity was found in the other groups (Figure 8B) at 2 weeks. Afterward, there was no osteoclasts activity observed in all the groups (data not shown).

4. DISCUSSION

In this study, we found that the biomimetic periosteum-covered β-TCP graft demonstrated significant vascularization and osteogenic potential, compared to the nonperiosteum/bone-like grafts. This result implies that spatial configuration of the biomimetic CSEP on the porous β-TCP scaffold has significant role in promoting the angiogenesis and osteogenesis. The spatial configuration of the CSEP is similar to the structure of native periosteum and shows associated function of periosteum.

We engineered this periosteum-like membrane based on a cell sheet engineering technique and integrated the membrane with a biodegradable porous β-TCP scaffold to form a periosteum-covered bone-like graft. Cell sheet engineering technique provides a potential to mimic the structure of periosteum. In this study, we used sharp pointed forceps to physically peel off and detach cell sheets from a culture dish instead of using a thermosensitive culture dish. Through this simple detaching technique, we first wrapped a mineralized hMSCs sheet on a

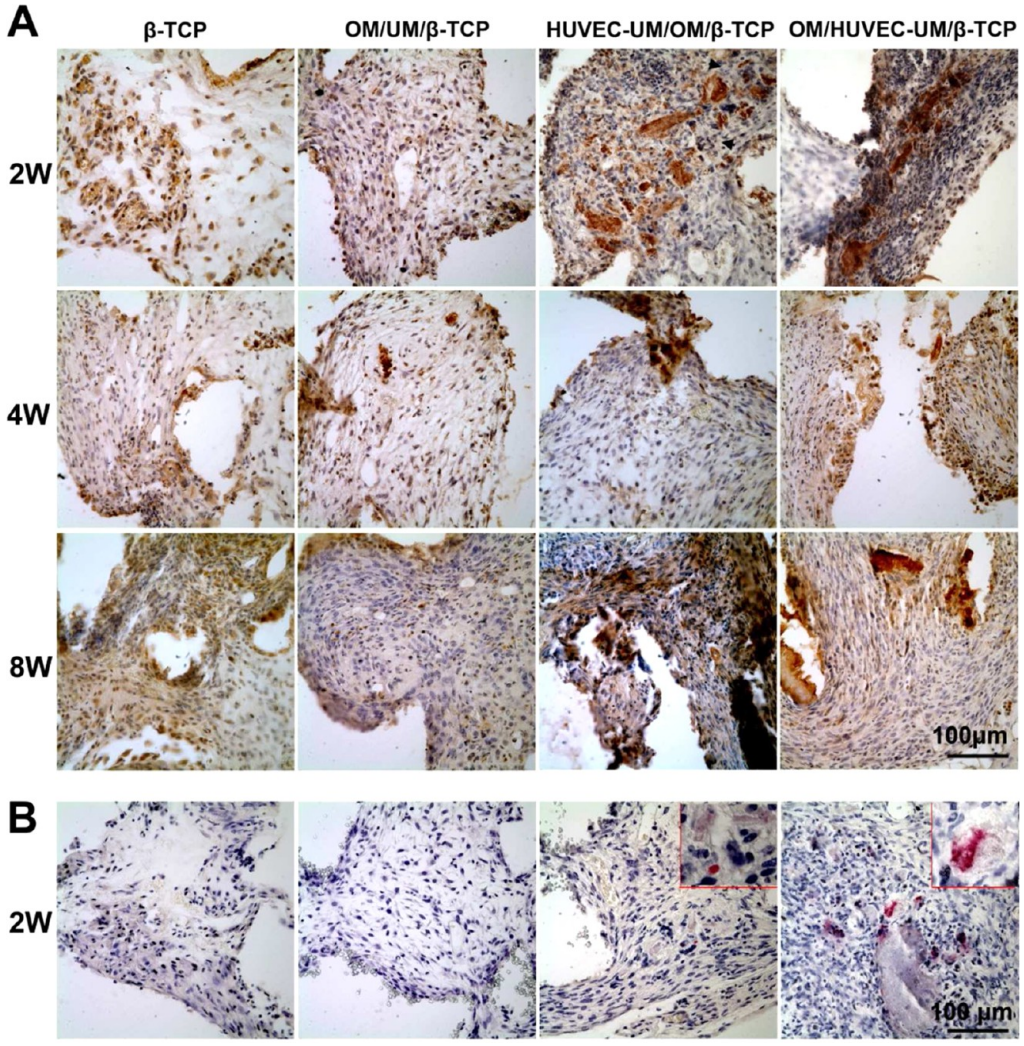

Figure 8. Immunohistochemistry staining of osteocalcin shows a denser osteocalcin matrix in HUVEC-UM/OM/β-TCP compared to those in other three groups at 2, 4, and 8 weeks (A); TRAP staining shows osteoclastic activity in the HUVEC-UM/OM/β-TCP and OM/HUVEC-UM/β-TCP at 2 weeks (B).

dx.doi.org/10.1021/am502056q | ACS Appl. Mater. Interfaces 2014, 6, 9622−9633

porous β-TCP scaffold, which mimicked the inner cambium layer of the native periosteum, followed by wrapping a prevascularized HUVEC/hMSC sheet onto the mineralized OM-covered scaffold, which mimicked the outer fibrous layer of the native periosteum.[23−25] The mechanical support of a rigid porous β-TCP scaffold is beneficial the sequential wrapping of two cell sheets and their integration, thus generating a biomimetic periosteum-covered bone-like graft. This strategy circumvents the limitations of using synthetic polymeric films or acellular human dermis in constructing a tissue-engineered periosteum. Synthetic polymeric films need cellularization for vascularization, and acellular human dermis also need revascularization.[46,47] Recently, more studies have reported the new progress in engineering periostea,[35−39] while in this study we used cell sheet to engineer biomimetic periosteum for vascularization. Single cell sheets can be further integrated with biodegradable porous scaffolds to form thick 3D constructs with biomimetic structure, which can provide robust tissue function and regeneration abilities.[48−54] Therefore, cell sheets combined with porous scaffolds has the potential to construct a tissue-engineered periosteum/bone-like graft with a more native structure and similar function.

The in vitro study results indicated that HUVECs migrated and formed robust networks on the undifferentiated hMSCs sheet. This implied that the cell sheet with rich ECM and intact proteins provide a microenvironment for cell migration, growth, and further neo-vascularization.[10,11,55] Similar results can be found in Soucy's study, which reported that a fibroblast-derived matrix promoted vasculogenic behavior of endothelial cells.[56] This result is very encouraging because HUVECs on the hMSCs sheet induced the development of blood vessel networks, and at the same time hMSCs may promote the stability of the new vessels and also provided an osteoblast source for bone formation when implanted in vivo.[57,58] The simultaneous migrations of both hMSCs and HUVECs from the outer CESP into the porous scaffold facilitate vascularization and osteogenesis. In our in vivo studies, H&E examination further confirmed that the grafts with a prevascularized sheet formed more blood vessels and attained a higher vessel density, compared to the plain scaffolds and OM/UM/β-TCP without the prevascularized cell sheet. This implies that the prevascularized cell sheet promoted the vascularization of the tissue-engineered grafts. Furthermore, we found that a greater number of functional perfused human blood vessels containing red blood cells formed in the periosteum-like group (HUVEC-UM/OM/β-TCP) than that formed in the non-periosteum-like group (OM/HUVEC-UM/β-TCP). This is probably a result of spatial structure of periosteum-like graft versus nonperiosteum-like graft. The outer prevascularized cell sheet layer of periosteum-like graft probably is closer to and easier to connect with the host vasculature, while in the nonperiosteum-like graft, the outer OM layer probably obstructed or slowed down the vessels from the inner prevascularized layer to reach and connect with the host vasculature, even though the thickness of the outer OM layer was at the scale of micrometers. There was a significant increase in new calcified osteoid matrix volume in the periosteum-like graft compared to the nonperiosteum-like graft and the others, suggesting the osteogenic capability of the CSEP. Therefore, this in vivo result suggests that CSEP mimics cellular components and the spatial structure of periosteum, potentially leading to a similar function.[29,59]

From H&E staining results we found that the vascular density declined from 2 to 8 weeks in all the groups. This result may be related to early immune response due to foreign implants, which caused the invasion of a large amount of vasculature at the early stage.[60,61] However, after the immune responses vanished and the newly formed vessels maturated, the number of vessels decreased.[62] Sun et al. observed a decrease of neovascular volume at the fracture site, and the relative number of erythrocytes decreased from 2 to 8 weeks.[60] Raines et al. found a decrease of neovascular volume in the marrow cavity after 2 weeks.[63] Risselada et al. also observed a time-dependent decline pattern of blood vessels.[62] Another study also showed that a larger number of vessel occurred from periphery to the cortex at the early stage, but they decreased in the later stages.[64] Our result is similar to these studies. Meanwhile, from the beginning of ossification to well-defined ossification, the metabolic activity of vessels also shows remarkable decay,[65] which may also decrease the osteoclast activity. This may be the reason that we observed the osteoclasts activities at 2 weeks and then disappeared afterward in our study. These results suggest that using autologous cells to develop cell sheet grafts may help avoid immune rejection responses.

The combination of CSEP and porous ceramic scaffold shows very encouraging results in vascularization and osteogenic potential and may bring very promising applications in reconstruction surgery. The porous scaffold provides structural support to the cell sheets and facilitates transplantation and handling in clinic use, while the cell sheets provide superior angiogenesis compared to grafts using only a porous synthetic scaffold. However, more studies need to be performed to investigate the anasotomosic mechanism of the prevascularized periosteum-like cell sheets with host vasculature to improve the in vitro prevascularization strategies. Although we preliminarily investigated the osteogenic potential of this CESP/β-TCP in ectopic subcutaneous sites, the osteogenic ability of this graft in orthotopic site will still need to be fully investigated and strengthen the findings of this study, and in that case, autograft or decellularized bone allograft may be involved as controls when implanted in situ bone defect. Also, in future studies, autologous cells from immunocompetent animals may be considered to be used to develop new periosteum/bone-like grafts for the applications of bone regeneration.

5. CONCLUSION

We constructed a biomimetic periosteum using hMSCs and HUVECs based on cell sheet engineering technique, and wrapped the CSEP on a porous, biodegradable β-TCP scaffold. This in vitro prevascularized biomimetic periosteum promoted the in vivo vascularization of β-TCP scaffold and possesses osteogenic potential. The cell sheet-ceramic complex with periosteum/bone-like structure provides a promising strategy not only mimicking the spatial configuration of native periosteum but also promoting the vascularization and osteogenic potential of bone grafts.

■ ASSOCIATED CONTENT

Ⓢ Supporting Information

Details of calculating the increased mineral bone volume in implants from MicroCT images. This material is available free of charge via the Internet at http://pubs.acs.org/.

■ AUTHOR INFORMATION

Corresponding Author

*Tel: 650-723-0772. Fax: 650-724-5401. Email: ypyang@stanford.edu.

Author Contributions

[‖]Y.K. and L.R. contributed equally to this work as cofirst authors. Y.K., L.R., and Y.Y. designed the experiments and wrote the manuscript. Y.K. and L.R. performed the experiments.

Notes

The authors declare no competing financial interest.

■ ACKNOWLEDGMENTS

This work was supported by grants from the following agencies: National Institutes of Health, NIH R01AR057837 (NIAMS), NIH R01DE021468 (NIDCR); Department of Defense, DOD W81XWH-10-1-0966 (PRORP); Wallace H. Coulter Foundation, National Natural Science Foundation of China (81170938, 81300860); and Chinese Fundamental Research Funds for the Central Universities (lzujbky-2013-173).

■ REFERENCES

(1) Schimming, R.; Schmelzeisen, R. Tissue-Engineered Bone for Maxillary Sinus Augmentation. *J. Oral Maxillofac. Surg.* **2004**, *62*, 724−729.

(2) Lattermann, C.; Romine, S. E. Osteochondral Allografts: State of the Art. *Clin. Sports Med.* **2009**, *28*, 285−301.

(3) Gitelis, S.; Cole, B. J. The Use of Allografts in Orthopaedic Surgery. *Instr. Course Lect.* **2002**, *51*, 507−520.

(4) Li, J.; Lin, Z.; Zheng, Q.; Guo, X.; Lan, S.; Liu, S.; Yang, S. Repair of Rabbit Radial Bone Defects Using True Bone Ceramics Combined with BMP-2-related Peptide and Type I Collagen. *Mater. Sci. Eng., C* **2010**, *30*, 1272−1279.

(5) Lozano, D.; Trejo, C. G.; Gomez-Barrena, E.; Manzano, M.; Doadrio, J. C.; Salinas, A. J.; Vallet-Regi, M.; Garcia-Honduvilla, N.; Esbrit, P.; Bujan, J. Osteostatin Loaded onto Mesoporous Ceramics Improves the Early Phase of Bone Regeneration in a Rabbit Osteopenia Model. *Acta Biomater.* **2012**, *8*, 2317−2323.

(6) Sprio, S.; Guicciardi, S.; Dapporto, M.; Melandri, C.; Tampieri, A. Synthesis and Mechanical Behavior of β-Tricalcium Phosphate/Titania Composites Addressed to Regeneration of Long Bone Segments. *J. Mech. Behav. Biomed. Mater.* **2013**, *17*, 1−10.

(7) Miño-Fariña, N.; Muñoz-Guzón, F. M.; López-Peña, M.; González-Cantalapiedra, A. Application of Different Calcium Phosphate Ceramics for Bone Regeneration. *Bone* **2011**, *48*, S168−S168.

(8) El-Ghannam, A. Bone Reconstruction: From Bioceramics to Tissue Engineering. *Expert. Rev. Med. Devices* **2005**, *2*, 87−101.

(9) Akita, S.; Tamai, N.; Myoui, A.; Nishikawa, M.; Kaito, T.; Takaoka, K.; Yoshikawa, H. Capillary Vessel Network Integration by Inserting a Vascular Pedicle Enhances Bone Formation in Tissue-Engineered Bone Using Interconnected Porous Hydroxyapatite Ceramics. *Tissue Eng.* **2004**, *10*, 789−795.

(10) Elcin, Y. M.; Dixit, V.; Gitnick, G. Extensive In Vivo Angiogenesis Following Controlled Release of Human Vascular Endothelial Cell Growth Factor: Implications for Tissue Engineering and Wound Healing. *Artif. Organs.* **2001**, *25*, 558−565.

(11) Royce, P. M.; Kato, T.; Ohsaki, K.; Miura, A. The Enhancement of Cellular Infiltration and Vascularization of a Collagenous Dermal Implant in the Rat by Platelet-derived Growth Factor BB. *J. Dermatol. Sci.* **1995**, *10*, 42−52.

(12) Chiu, L. L.; Radisic, M. Scaffolds with Covalently Immobilized VEGF and Angiopoietin-1 for Vascularization of Engineered Tissues. *Biomaterials* **2010**, *31*, 226−241.

(13) Freeman, I.; Cohen, S. The Influence of the Sequential Delivery of Angiogenic Factors from Affinity-binding Alginate Scaffolds on Vascularization. *Biomaterials* **2009**, *30*, 2122−2131.

(14) Geiger, F.; Lorenz, H.; Xu, W.; Szalay, K.; Kasten, P.; Claes, L.; Augat, P.; Richter, W. VEGF Producing Bone Marrow Stromal Cells (BMSC) Enhance Vascularization and Resorption of a Natural Coral Bone Substitute. *Bone* **2007**, *41*, 516−522.

(15) Anderson, S. M.; Siegman, S. N.; Segura, T. The Effect of Vascular Endothelial Growth Factor (VEGF) Presentation within Fibrin Matrices on Endothelial Cell Branching. *Biomaterials* **2011**, *32*, 7432−7443.

(16) Fuchs, S.; Ghanaati, S.; Orth, C.; Barbeck, M.; Kolbe, M.; Hofmann, A.; Eblenkamp, M.; Gomes, M.; Reis, R. L.; Kirkpatrick, C. J. Contribution of Outgrowth Endothelial Cells from Human Peripheral Blood on In Vivo Vascularization of Bone Tissue Engineered Constructs Based on Starch Polycaprolactone Scaffolds. *Biomaterials* **2009**, *30*, 526−534.

(17) Kirkpatrick, C. J.; Fuchs, S.; Unger, R. E. Co-culture Systems for Vascularization—Learning from Nature. *Adv. Drug Delivery Rev.* **2011**, *63*, 291−299.

(18) Novosel, E. C.; Kleinhans, C.; Kluger, P. J. Vascularization is the Key Challenge in Tissue Engineering. *Adv. Drug Delivery Rev.* **2011**, *63*, 300−311.

(19) Kang, Y.; Kim, S.; Fahrenholtz, M.; Khademhosseini, A.; Yang, Y. Osteogenic and Angiogenic Potentials of Monocultured and Co-cultured Human-Bone-Marrow-Derived Mesenchymal Stem Cells and Human-Umbilical-Vein Endothelial Cells on Three-Dimensional Porous β-Tricalcium Phosphate Scaffold. *Acta Biomater.* **2013**, *9*, 4906−4915.

(20) Wang, L.; Fan, H.; Zhang, Z. Y.; Lou, A. J.; Pei, G. X.; Jiang, S.; Mu, T. W.; Qin, J. J.; Chen, S. Y.; Jin, D. Osteogenesis and Angiogenesis of Tissue-Engineered Bone Constructed by Prevascularized β-Tricalcium Phosphate Scaffold and Mesenchymal Stem Cells. *Biomaterials* **2010**, *31*, 9452−9461.

(21) Kokemueller, H.; Spalthoff, S.; Nolff, M.; Tavassol, F.; Essig, H.; Stuehmer, C.; Bormann, K. H.; Rücker, M.; Gellrich, N. C. Prefabrication of Vascularized Bioartificial Bone Grafts In Vivo for Segmental Mandibular Reconstruction: Experimental Pilot Study in Sheep and First Clinical Application. *Int. J. Oral Maxillofac. Surg.* **2010**, *39*, 379−387.

(22) Altun, B. U. Periosteum: Resorption or Formation Area? *Turk. Jem.* **2008**, *12*, 28−31.

(23) Knothe Tate, M. L. "Whither Flows the Fluid in Bone?" An Osteocyte's Perspective. *J. Biomech.* **2003**, *36*, 1409−1424.

(24) Tami, A. E.; Schaffler, M. B.; Knothe Tate, M. L. Probing the Tissue to Subcellular Level Structure Underlying Bone's Molecular Sieving Function. *Biorheology* **2003**, *40*, 577−590.

(25) Evans, S. F.; Parent, J. B.; Lasko, C. E.; Zhen, X.; Knothe, U. R.; Lemaire, T.; Knothe Tate, M. L. Periosteum, Bone's "Smart" Bounding Membrane, Exhibits Direction-Ddependent Permeability. *J. Bone Miner. Res.* **2013**, *28*, 608−617.

(26) Song, H. R.; Puri, A.; Lee, J. H.; Park, H. B.; Ra, D. K.; Kim, G. S.; Yeon, S. C. Spontaneous Bone Regeneration in Surgically Induced Bone Defects in Young Rabbits. *J. Pediatr. Orthop. B* **2002**, *11*, 343−349.

(27) Chen, X.; Aledia, A. S.; Ghajar, C. M.; Griffith, C. K.; Putnam, A. J.; Hughes, C. C.; George, S. C. Prevascularization of a Fibrin-based Ttissue Construct Accelerates the Formation of Functional Anastomosis with Host Vasculature. *Tissue Eng., Part A* **2009**, *15*, 1363−1371.

(28) Runyan, C. M.; Jones, D. C.; Bove, K. E.; Maercks, R. A.; Simpson, D. S.; Taylor, J. A. Porcine Allograft Mandible Revitalization Using Autologous Adipose-derived Stem Cells, Bone Morphogenetic Protein-2, and Periosteum. *Plast. Reconstr. Surg.* **2010**, *125*, 1372−1382.

(29) Canalis, R. F.; Burstein, F. D. Osteogenesis in Vascularized Periosteum. Interactions with Underlying Bone. *Arch. Otolaryngol.* **1985**, *111*, 511−516.

(30) Maercks, R. A.; Runyan, C. M.; Jones, D. C.; Taylor, J. A. The Vastus Intermedius Periosteal (VIP) Flap: A Novel Flap for Osteoinduction. *J. Reconstr. Microsurg.* **2010**, *26*, 335−340.

(31) Iorio, M. L.; Masden, D. L.; Higgins, J. P. The Limits of Medial Femoral Condyle Corticoperiosteal Flaps. *J. Hand Surg. Am.* **2011**, *36*, 1592−1596.

(32) Gallay, S. H.; Miura, Y.; Commisso, C. N.; Fitzsimmons, J. S.; O'Driscoll, S. W. Relationship of Donor Site to Chondrogenic Potential of Periosteum In Vitro. *J. Orthop. Res.* **1994**, *12*, 515−525.

(33) Zhao, L.; Zhao, J.; Wang, S.; Wang, J.; Liu, J. Comparative Study Between Tissue-Engineered Periosteum and Structural Allograft in

Rabbit Critical-Sized Radial Defect Model. *J. Biomed. Mater. Res., Part B* **2011**, *97*, 1−9.
(34) Schonmeyr, B.; Clavin, N.; Avraham, T.; Longo, V.; Mehrara, B. J. Synthesis of a Tissue-Engineered Periosteum with Acellular Dermal Matrix and Cultured Mesenchymal Stem Cells. *Tissue Eng., Part A* **2009**, *15*, 1833−1841.
(35) Long, T.; Zhu, Z.; Awad, H. A.; Schwarz, E. M.; Hilton, M. J.; Dong, Y. The Effect of Mesenchymal Stem Cell Sheets on Structural Allograft Healing of Critical Sized Femoral Defects in Mice. *Biomaterials* **2014**, *35*, 2752−2759.
(36) Shi, X.; Chen, S.; Zhao, Y.; Lai, C.; Wu, H. Enhanced Osteogenesis by a Biomimic Pseudo-periosteum-Involved Tissue Engineering Strategy. *Adv. Healthcare Mater.* **2013**, *2*, 1229−1235.
(37) Hoffman, M. D.; Xie, C.; Zhang, X.; Benoit, D. S. The Effect of Mesenchymal Stem Cells Delivered via Hydrogel-based Tissue Engineered Periosteum on Bone Allograft Healing. *Biomaterials* **2013**, *34*, 8887−8898.
(38) Xie, C.; Reynolds, D.; Awad, H.; Rubery, P. T.; Pelled, G.; Gazit, D.; Guldberg, R. E.; Schwarz, E. M.; O'Keefe, R. J.; Zhang, X. Structural Bone Allograft Combined with Genetically Engineered Mesenchymal Stem Cells as a Novel Platform for Bone Tissue Engineering. *Tissue Eng.* **2007**, *13*, 435−445.
(39) Zhang, X.; Xie, C.; Lin, A. S.; Ito, H.; Awad, H.; Lieberman, J. R.; Rubery, P. T.; Schwarz, E. M.; O'Keefe, R. J.; Guldberg, R. E. Periosteal Progenitor Cell Fate in Segmental Cortical Bone Graft Transplantations: Implications for Functional Tissue Engineering. *J. Bone Miner. Res.* **2005**, *20*, 2124−2137.
(40) Nehls, V.; Denzer, K.; Drenckhahn, D. Pericyte Involvement in Capillary Sprouting During Angiogenesis In Situ. *Cell Tissue Res.* **1992**, *270*, 469−474.
(41) Adams, R. H.; Alitalo, K. Molecular Regulation of Angiogenesis and Lymphangiogenesis. *Nat. Rev. Mol. Cell Biol.* **2007**, *8*, 464−478.
(42) Liu, Y.; Kim, J. H.; Young, D.; Kim, S.; Nishimoto, S. K.; Yang, Y. Novel Template-Casting Technique for Fabricating β-Tricalcium Phosphate Scaffolds with High Interconnectivity and Mechanical Strength and In Vitro Cell Responses. *J. Biomed. Mater. Res., Part A* **2010**, *92*, 997−1006.
(43) Kang, Y.; Kim, S.; Khademhosseini, A.; Yang, Y. Creation of Bony Microenvironment with CaP and Cell-Derived ECM to Enhance Human Bone-Marrow MSC Behavior and Delivery of BMP-2. *Biomaterials* **2011**, *32*, 6119−6130.
(44) Kang, Y.; Scully, A.; Young, D. A.; Kim, S.; Tsao, H.; Sen, M.; Yang, Y. Enhanced Mechanical Performance and Biological Evaluation of a PLGA Coated Beta-TCP Composite Scaffold for Load-Bearing Applications. *Eur. Polym. J.* **2011**, *47*, 1569−1577.
(45) Kang, Y.; Kim, S.; Bishop, J.; Khademhosseini, A.; Yang, Y. The Osteogenic Differentiation of Human Bone Marrow MSCs on HUVEC-Derived ECM and β-TCP Scaffold. *Biomaterials* **2012**, *33*, 6998−7007.
(46) Bauer, S. M.; Bauer, R. J.; Liu, Z. J.; Chen, H.; Goldstein, L.; Velazquez, O. C. Vascular Endothelial Growth Factor-C Promotes Vasculogenesis, Angiogenesis, and Collagen Constriction in Three-Dimensional Collagen Gels. *J. Vasc. Surg.* **2005**, *41*, 699−707.
(47) Eppley, B. L. Experimental Assessment of the Revascularization of Acellular Human Dermis for Soft-Tissue Augmentation. *Plast. Reconstr. Surg.* **2001**, *107*, 757−762.
(48) Ma, D.; Yao, H.; Tian, W.; Chen, F.; Liu, Y.; Mao, T.; Ren, L. Enhancing Bone Formation by Transplantation of a Scaffold-free Tissue-Engineered Periosteum in a Rabbit Model. *Clin. Oral Implants Res.* **2011**, *22*, 1193−1199.
(49) Ma, D.; Zhong, C.; Yao, H.; Liu, Y.; Chen, F.; Li, J.; Zhao, J.; Mao, T.; Ren, L. Engineering Injectable Bone Using Bone Marrow Stromal Cell Aggregates. *Stem Cells Dev.* **2011**, *20*, 989−999.
(50) Ma, D.; Ren, L.; Chen, F.; Liu, Y.; Zhang, J.; Xue, Z.; Mao, T. Reconstruction of Rabbit Critical-size Calvarial Defects Using Autologous Bone Marrow Stromal Cell Sheets. *Ann. Plast. Surg.* **2010**, *65*, 259−265.
(51) Ren, L.; Kang, Y. Q.; Browne, C.; Bishop, J.; Yang, Y. Fabrication, Vascularization, and Osteogenic Properties of a Novel Synthetic Biomimetic Induced Membrane for the Treatment of Large Bone Defects. *Bone* **2014**, *64*, 173−182.
(52) Ma, D.; Ren, L.; Yao, H.; Tian, W.; Chen, F.; Zhang, J.; Liu, Y.; Mao, T. Locally Injection of Cell Sheet Fragments Enhances New Bone Formation in Mandibular Distraction Osteogenesis: A Rabbit Model. *J. Orthop. Res.* **2013**, *31*, 1082−1088.
(53) Yuan, Q.; Kubo, T.; Doi, K.; Morita, K.; Takeshita, R.; Katoh, S.; Shiba, T.; Gong, P.; Akagawa, Y. Effect of Combined Application of bFGF and Inorganic Polyphosphate on Bioactivities of Osteoblasts and Bone Regeneration. *Acta Biomater.* **2009**, *5*, 1716−1724.
(54) Elloumi-Hannachi, I.; Yamato, M.; Okano, T. Cell Sheet Engineering: A Unique Nanotechnology for Scaffold-free Tissue Reconstruction with Clinical Applications in Regenerative Medicine. *J. Int. Med.* **2010**, *267*, 54−70.
(55) Chalupowicz, D. G.; Chowdhury, Z. A.; Bach, T. L.; Barsigian, C.; Martinez, J. Fibrin II Induces Endothelial Cell Capillary Tube Formation. *J. Cell. Biol.* **1995**, *130*, 207−215.
(56) Soucy, P. A.; Romer, L. H. Endothelial Cell Adhesion, Signaling, and Morphogenesis in Fibroblast-Derived Matrix. *Matrix Biol.* **2009**, *28*, 273−283.
(57) Mendes, L. F.; Pirraco, R. P.; Szymczyk, W.; Frias, A. M.; Santos, T. C.; Reis, R. L.; Marques, A. P. Perivascular-like Cells Contribute to the Stability of the Vascular Network of Osteogenic Tissue Formed from Cell Sheet-based Constructs. *PLoS One* **2012**, *7*, 1−12.
(58) Blocki, A.; Wang, Y.; Koch, M.; Peh, P.; Beyer, S.; Law, P.; Hui, J.; Raghunath, M. Not All MSCs can Act as Pericytes: Functional In Vitro Assays to Distinguish Pericytes from other Mesenchymal Stem Cells in Angiogenesis. *Stem Cells Dev.* **2013**, *22*, 2347−2355.
(59) Yachouh, J.; Breton, P.; Roux, J. P.; Goudot, P. Osteogenic Capacity of Vascularized Periosteum: An Experimental Study on Mandibular Irradiated Bone in Rabbits. *J. Plast. Reconstr. Aesthet. Surg.* **2010**, *63*, 2160−2167.
(60) Sun, M. H.; Leung, K. S.; Zheng, Y. P.; Huang, Y. P.; Wang, L. K.; Qin, L.; Leung, A. H.; Chow, S. K.; Cheung, W. H. Three-Dimensional High Frequency Power Doppler Ultrasonography for the Assessment of Microvasculature during Fracture Healing in a Rat Model. *J. Orthop. Res.* **2012**, *30*, 137−143.
(61) Kollmann, C.; Turetschek, K.; Mostbeck, G. Amplitude-coded Colour Doppler Sonography: Physical Principles and Technique. *Eur. Radiol.* **1998**, *8*, 649−656.
(62) Risselada, M.; Kramer, M.; Saunders, J. H.; Verleyen, P.; Van Bree, H. Power Doppler Assessment of the Neovascularization during Uncomplicated Fracture Healing of Long Bones in Dogs and Cats. *Vet. Radiol. Ultrasound* **2006**, *47*, 301−306.
(63) Raines A. L., S M., Thacker K. Angiogenesis in Hyaluronan Treated Bone Repair. *56th Annual Meeting of the Orthopaedic Research Society* **2010**, March, New Orleans.
(64) Bottinelli, O.; Calliada, F.; Campani, R. Bone Callus: Possible Assessment with Color Doppler Ultrasonography. Normal Bone Healing Process. *Radiol. Med.* **1996**, *91*, 537−541.
(65) Barros, J. W.; Barbieri, C. H.; Fernandes, C. D. Scintigraphic Evaluation of Tibial Shaft Fracture Healing. *Injury* **2000**, *31*, 51−54.